Composite Proton Exchange Membranes from Zirconium-Based Solid Acids and PVDF/Acrylic Polyelectrolyte Blends

Pedro Zapata, Jung-Hyun Lee, J. Carson Meredith

School of Chemical and Biomolecular Engineering, Georgia Institute of Technology, Atlanta, Georgia 30332-0100

Received 24 May 2011; accepted 1 October 2011
DOI 10.1002/app.36275
Published online 20 January 2012 in Wiley Online Library (wileyonlinelibrary.com).

ABSTRACT: Organic–inorganic composite proton exchange membranes (PEMs) are of interest in fuel cell applications because of potential benefits in conductivity, mechanical, and transport properties that may be imparted by the inorganic component. Our previous work showed that polymeric membranes based on blends of poly(vinylidene fluoride) (PVDF) and cross-linked sulfonated acrylic polyelectrolytes (PE) compare favorably against the proton conductivity and mechanical properties of commercial perfluorosulfonic acid-based PEMs. One problem found in the previous study was that crystalline regions in homopolymers of PVDF interfered with the formation of proton conducting pathways by the PE component. In this study, we explore the ability to use proton-conductive zirconium-based inorganic particles to improve conductivity in such PVDF/PE membranes. Three different particles were considered, namely, zirconium oxide, zirconium hydroxide sulfate, and zirconium hydrogen phosphate. Dispersion of particles in the polymer matrix was limited, resulting in severe aggregation at particle loadings above 5 wt %. Nevertheless, a general improvement in proton conductivity was evidenced in composite membranes with 0.5 to 1 wt % particle loadings. This beneficial effect was particularly noticeable in membranes manufactured from highly crystalline PVDF homopolymers (7 to 14% increase). We propose that the surface of zirconium particles act to provide proton conducting pathways between PE regions that otherwise would become blocked due to PVDF crystallization. In addition to conductivity, composite membranes exhibited enhancement of tensile properties at identical particle loadings, especially in membranes containing more flexible PVDF:HFP copolymers, where a reinforcing stiffening effect was evident (19 to 22% elastic modulus increment). J Appl Polym Sci 124: E241–E250, 2012

Key words: zirconium; composites; proton exchange membrane; fuel cells; PVDF

INTRODUCTION

The proton exchange membrane fuel cell (PEMFC) is a promising alternative to provide power for mobile and stationary applications.[1–4] One of the key components of the PEMFC is the polymer electrolyte or proton exchange membrane (PEM). The PEM is a proton-conducting polymeric solid that provides proton transport between the anode and the cathode, while simultaneously serving as a barrier to prevent crossover between the fuel and oxidant streams. Besides proton transport and gas barrier properties, the PEM needs to satisfy other essential requirements for the appropriate operation of the fuel cell, including low electronic conductivity, low water transport, high hydrolytic stability, and excellent mechanical integrity, among several others.[5,6]

A large research effort has focused on developing cost-effective PEM materials with the purpose of closing the breach between existing PEMFC technology [based primarily on perfluorosulfonic acid (PFSA) membranes[3–5]] and commercialization targets (e.g., DOE targets for portable fuel cells[4]). Numerous approaches are being considered in the development of these new PEM materials, including modification of PFSA-based membranes, functionalization of high-performance hydrocarbon polymers, polymer blends of inert and ionic conductive precursors, and organic/inorganic composite membranes, just to mention a few.[5,7–11] Among these, organic/inorganic composite or hybrid PEMs have gained attention because of the potential beneficial effects of introducing inorganic fillers in the polymer matrix.[9–20]

Inorganic candidate materials include metal oxides (e.g., SiO_2, TiO_2, ZrO_2, and Al_2O_3),[9,10,12] solid acids such as sulfates and phosphates,[9,11–13,17–19,21] and nanoclays (e.g., montmorillonite).[20] Among these, solid acids appear to have considerable potential because of their proton-conducting properties and

Additional Supporting Information may be found in the online version of this article.

Correspondence to: J. C. Meredith (carson.meredith@chbe.gatech.edu).

hydrophilicity.[6,9,13] Of particular interest are tetravalent metal acids based on zirconium, particularly zirconium phosphate,[11,13,15,16,22] which can preserve its proton conductivity up to 300°C,[6] and sulfated zirconia,[12,17] which is one of the strongest solid superacids known and can retain sulfonic acid groups responsible for proton conduction up to 500°C.[12,23]

Recently, PEMs from semi-interpenetrating networks of PVDF and cross-linked sulfonated acrylic polyelectrolytes (PEs) were studied and characterized.[8,24] These PVDF/PE blended membranes exhibited proton conducting and mechanical properties comparable to or exceeding Nafion® standards. Here, we examine the possibility of improving these properties even further by incorporating zirconium-based fillers (i.e., zirconium oxide, zirconium hydrogen phosphate, and zirconium hydroxide sulfate) into the polymer blend to produce organic/organic/inorganic triphase PEMs. High-throughput characterization tools are used to assess the proton conductivity and mechanical properties of the PVDF/PE zirconium-based composite membranes.

EXPERIMENTAL

Composite membrane synthesis and protonation

Composite membranes were prepared by mixing zirconium-based particles with blends of five Kynar® PVDF grades and a sulfonated acrylic polyelectrolyte (PE).[8,25] The PE consists of a random copolymer of 2-sulfoethyl methacrylate (SEM) (~ 69 wt %), 2-hydroxyethyl methacrylate (HEMA) (~ 15 wt %), methyl methacrylate (MMA) (~ 8 wt %), and styrene (~ 7 wt %); and has an equivalent mass of 280 g PE/mol SO_3H. Two PVDF homopolymers, one with approximately twice the molecular mass of the other (Kynar® 500 and Kynar® 731), and three random copolymers of vinylidene fluoride and hexafluoropropylene (HFP) (Kynar® 2801, Kynar® 2821, and Kynar® 2851), which vary the relative amount of HFP, have been chosen. The variation in molecular mass and HFP content leads to differences in crystallinity, glass transition temperature, and crystallite size that are expected to influence the formation of proton conducting channels in blends with PEs. The different Kynar® PVDF grades utilized were Kynar® 500 (M_w = 523,000 g/mol; H—H defect = 11.6%), Kynar® 731 (M_w = 260,000 g/mol; H—H defect = 10%), Kynar® 2801 (M_w = 380,000 g/mol; PVDF:HFP = 88 : 12 molar ratio), Kynar® 2821 (PVDF:HFP = 88 : 12 molar ratio), and Kynar® 2851 (M_w = 455,000 g/mol; PVDF:HFP=95 : 5 molar ratio), all in a fine powder form (supplied by Arkema Inc., Kynar® is a registered trademark of Arkema Inc.).[8,25] PVDF was dissolved in 1-methyl-2-pyrrolidinone (NMP) (Sigma–Aldrich Co., assay ≥99.5%) to a total concentration of 10 wt % per solution. These PVDF solutions were mixed with a stock solution of the PE (25 wt % total solids in NMP) at a fixed mass ratio (dry base) of 65 : 35 (PVDF:PE, acid form). Three different types of zirconium-based particles were utilized; namely, zirconium(IV) oxide nanopowder (ZrO_2) (particle size <100 nm), zirconium(IV) hydroxide sulfate ($Zr(H_2SO_4)_4$), and zirconium(IV) hydrogen phosphate ($Zr(HPO_4)_2$) (Sigma–Aldrich Co.). The size of the mesoporous zirconium(IV) hydroxide sulfate and zirconium(IV) hydrogen phosphate particles was further reduced by crushing them using a zirconia mortar and pestle. Final particle size was ~ 100 to 300 nm for zirconium(IV) hydroxide sulfate and 200–1000 nm for zirconium(IV) hydrogen phosphate. For the remainder of this work zirconium oxide, sulfated zirconium hydroxide, and zirconium hydrogen phosphate will be referred to as ZrO, ZrS, and ZrHP, respectively. Before mixing with the PVDF/PE blends, the particles were suspended in NMP by vigorous stirring for 6 h, followed by overnight sonication in an ultrasonic bath, and 20 min "strong" sonication using a horn-type sonicator. Each particle suspension type was mixed with every PVDF/PE blend at 0.5 (low), 1 (medium), and 5 wt % (high) to give a total of 45 different mixtures (in addition to five reference PVDF/PE blends without particles). The PVDF/PE/ZrX (X = O, S, HP) mixtures were combined with Desmodur N-3300A (Bayer AG.), a 1,6-hexamethylene diisocyanate-derived triisocyanate cross-linker, at a 1 : 0.8 OH:NCO ratio (80 mol % of the stoichiometric amount of cross-linker needed to react with all the PE hydroxyl groups). The final blends were thoroughly mixed at room temperature under an inert nitrogen atmosphere for ~ 30 min, followed by a degassing and redispersion of the particles by sonication (~ 15 min) immediately before film coating. Coating was performed using a knife-edge apparatus[26] to spread liquid PVDF/PE/ZrX films onto silicon <100> substrates (Silicon, Inc.) previously cleaned for 2 h in Piranha solution (70% H_2SO_4, 9% H_2O_2, and 21% H_2O) at 80°C. The resulting films were cured at 175°C for 20 min in a forced air convection oven to cross-link the PE and remove excess NMP. Cured composite membranes were detached from the silicon substrates by immersion in DI water at room temperature.

Before protonation, free-standing composite membranes were washed in a 1.0*M* HCl solution at 80°C for 2 h, followed by a 15-min rinse in DI water. The acid-washed membranes were protonated by immersion in 1*M* H_2SO_4 at 80°C for 2 h, followed by removal of excess sulfuric acid by several successive 15-min rinses in DI water until the pH of the rinse water was above 4. Conditioning of protonated composite membranes, as well as particle-free PVDF/PE references, was carried out by immersion in boiling

18.2 MΩ water for 1 h to allow complete membrane swelling. Swollen membranes were stored in 18.2 MΩ water until conductivity and mechanical property measurements were performed.

Membrane characterization

Proton conductivity measurements were performed by AC electrochemical impedance spectroscopy (EIS) using a custom, automated 4-point probe high-throughput conductivity measuring device (HTC).[24] Conductivity measurements in 18.2 MΩ water at ~ 25°C were performed in potentiostatic mode with an excitation signal of 1000 Hz and 30 mV (~ 20 mV RMS).

Characterization of mechanical properties was carried out using a high-throughput mechanical testing apparatus (HTMECH)[8,25] at a constant speed of 10 mm/s using a 1.24 mm diameter needle. All membranes were tested in a fully hydrated state. It is important to note that contrary to uniaxial deformation, typical of conventional mechanical characterization, membranes undergo axisymmetric biaxial deformation in HTMECH tests. Therefore, care must be taken if the results presented herein are to be compared to uniaxial tensile tests, as differences in mechanical response are expected between both deformation models.

X-ray diffraction spectra of composite membranes and particle powders were recorded using a PANalytical X'Pert PRO diffractometer (PANalytical). The incident beam configuration consisted of a Cu-anode tube (λ CuKα_1 = 1.540598 Å, λ CuKα_2 = 1.544426 Å) operated at 45 kV and 40 mA with a fixed 1/16°(0.19 mm) divergence slit, a 0.04 rad Soller slit, and a nickel β-filter to remove CuKβ radiation. The detector, a PANalytical X'Celerometer, was equipped with a 10 mm anti-scatter slit and a 0.04 rad Soller slit. Data were collected over a 2θ range of 1°–65° using a step size of 0.033°.

Infrared absorption spectra of composite membranes were collected at room temperature with a Bruker Equinox 55 FTIR spectrometer (Bruker Optics Inc.) coupled with a KBr beam splitter. The spectra were recorded in the range of 400–5000 cm^{-1} at a resolution of 4 cm^{-1} and averaged 128 times.

High resolution images of the cross-sectional area of composite membranes were obtained using a LEO 1530 thermally assisted field emission scanning electron microscope (LEO Electron Microscopy Group), operated at 10 keV. Membrane samples for SEM imaging where prepared by cryogenic breaking in liquid nitrogen followed by vacuum metallization with gold.

Statistical analysis

To provide an ability to distinguish effects of various compositions, over 300 independent sample films were prepared in total. An unbalanced univariate general linear model (GLM) (two and three-way, type III sums of squares) was used for evaluation of significant factors with $P < 0.05$ defined as significant. Pairwise comparisons of significant factors from three-way GLM tests were performed by comparisons of unweighted means of main effects with Sidak-adjusted confidence intervals, whereas Tamhane's T2 post hoc test was utilized for pairwise comparisons of significant factors from two-way GLM tests. All results are expressed as mean ± standard error of the mean (± S.E.M.) or as mean ±95% confidence intervals, as indicated.

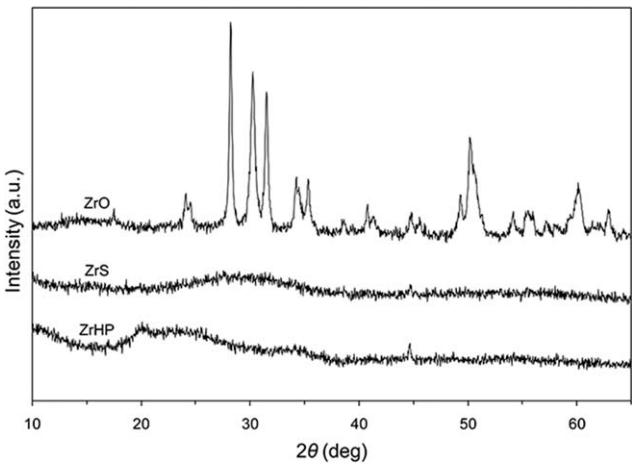

Figure 1 Wide angle X-ray diffraction spectra of ZrO, ZrS, and ZrHP particle powders.

RESULTS AND DISCUSSION

Microstructure of composite membranes

X-ray diffraction spectra of the three zirconium-based powders are shown in Figure 1. The crystalline reflections (Bragg peaks) in the zirconia (ZrO) spectrum, particularly those located at scattering angles (2θ) of 28.2°, 30.2°, and 31.5°, indicate a mixed crystalline form of monoclinic and tetragonal ZrO phases.[23,27] In contrast, ZrHP and ZrS are characterized by an amorphous halo with absence of crystalline reflections. In the case of ZrHP, the amorphous spectrum indicates a disordered layer aggregation, and thus, the absence of lamellar α-ZrHP and/or γ-ZrHP. From a practical point of view, this may be beneficial for the overall proton conductivity of ZrHP-based composite membranes, as amorphous ZrHP exhibits higher conductivity than comparable crystalline and semicrystalline α-ZrHP and γ-ZrHP (1–5 × 10^{-3} vs. 1.8 × 10^{-5} and 2 × 10^{-4} S/cm at 100°C and 95%RH, respectively[21]). Similarly, conductivity of membranes based on amorphous ZrS could potentially benefit from a larger number of surface acid sites exposed, given that amorphous

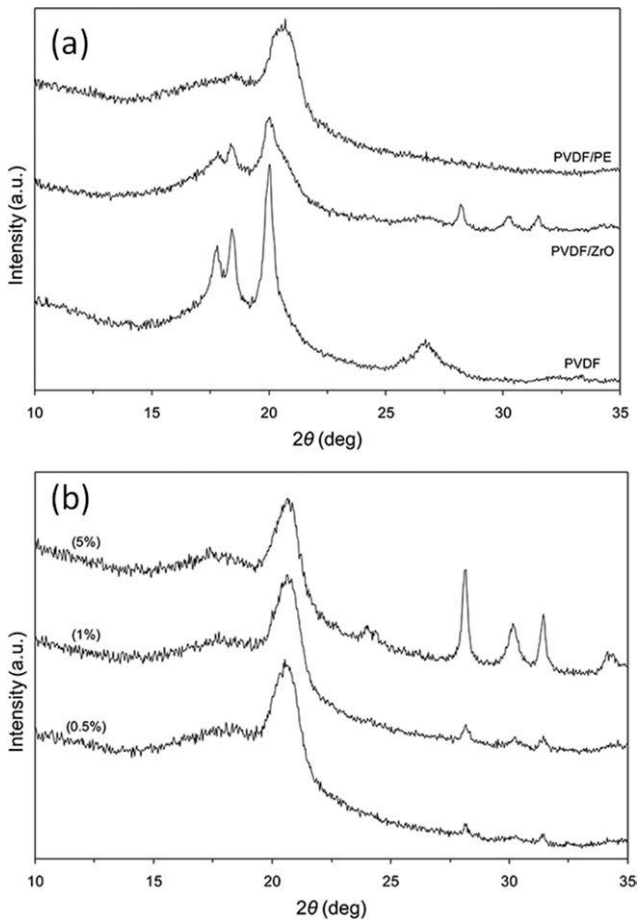

Figure 2 Wide angle X-ray diffraction spectra of (a) pure and modified PVDF films, and (b) composite membranes with different particle loadings. All the spectra correspond to Kynar® 731-based films (other PVDF grades exhibited identical behavior). The representative spectra of the particle modified PVDF film and the composite membranes correspond to ZrO.

materials generally exhibit larger surface area than crystalline counterparts.[28]

It has been shown that polymer characteristics, such as crystalline structure, can be affected by salt or acid complexation and/or incorporation of inorganic fillers.[29,30] The crystalline structure of membranes was analyzed by X-ray diffraction (Fig. 2). The crystalline reflections in the spectrum of pristine solvent-cast PVDF films, prepared at identical conditions as the composite membranes, at scattering angles (2θ) of 17.8°, 18.4°, 19.9°, and 26.6° indicate a predominant crystalline α-phase.[8,31] An apparent decline in the crystallinity of the PVDF by incorporation of zirconium-based particles may be inferred from the reduced intensity and broadening of the Bragg peaks in binary PVDF/ZrX controls. However, a shoulder to the right of the 19.9° Bragg peak indicates the formation of β-phase PVDF crystals in presence of ZrX and thus suggests that the change in the PVDF spectrum with the addition of the ZrX particles arises mainly from a mixture of α- and β-phase PVDF. This is confirmed by the appearance of distinctive β-phase absorption bands at 510 cm^{-1} and a ferroelectric all-trans conformation CF_2 bending[8,32] at 842 cm^{-1} in the FTIR spectra of the binary control samples (Fig. 3). Addition of PE to the PVDF matrix results in a complete paraelectric to ferroelectric transition of the PVDF crystalline phase characterized by a crystalline reflection at (2θ) 20.6°,[8,31] and confirmed by the disappearance of the nonpolar trans-gauche CF_2 bending band at 532 cm^{-1} in the FTIR of the PVDF/PE membrane spectrum. In summary, the incorporation of either PE or ZrX into the PVDF matrix disturbs the PVDF crystalline structure by inducing α- to β-phase transitions; as a result, the β-phase polymorph is prevalent in the PVDF support matrix of the composite membranes, as seen in Figure 2(b). The diffraction peaks at 28.2°, 30.2°, and 31.5° in the representative XRD spectra of composite membranes correspond to ZrO particles embedded in the polymer matrix. The intensity variation of these crystalline reflections is a clear indicator of different particle loadings. Small angle X-ray diffraction measurements of the zirconium-based additives (not shown) revealed no mesostructure and no basal plane diffraction peaks, in agreement with the amorphous structure of ZrHP and ZrS, and indicating a nonlamellar structure for the crystalline ZrO. (Alternatively, if a lamellar structure does exist, the interlayer distance exceeds the largest layered spacing that can be determined by the X-ray diffractometer).

A foremost concern when preparing polymeric composites is the dispersion of the inorganic phase within the polymer matrix. Consequently, SEM imaging was used to assess the dispersion of the

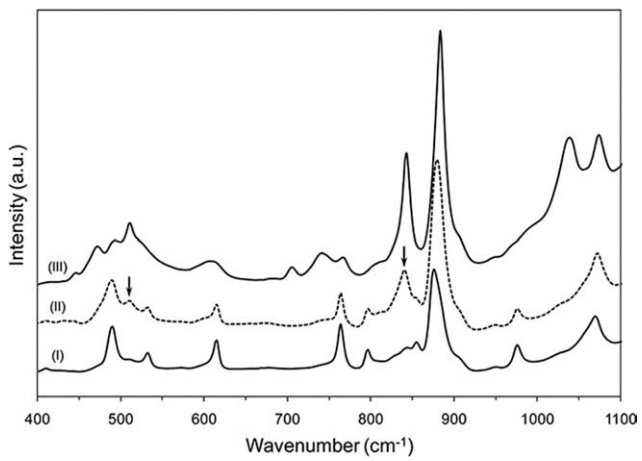

Figure 3 FTIR spectra in the range of 400–1100 cm^{-1} corresponding to the pure and modified PVDF films shown in Figure 2a: (I) PVDF, (II) PVDF/ZrO, and (III) PVDF/PE. The arrows indicate the appearance of characteristic PVDF β-phase bands at 510 cm^{-1} and 842 cm^{-1} as a result of the incorporation of particles.

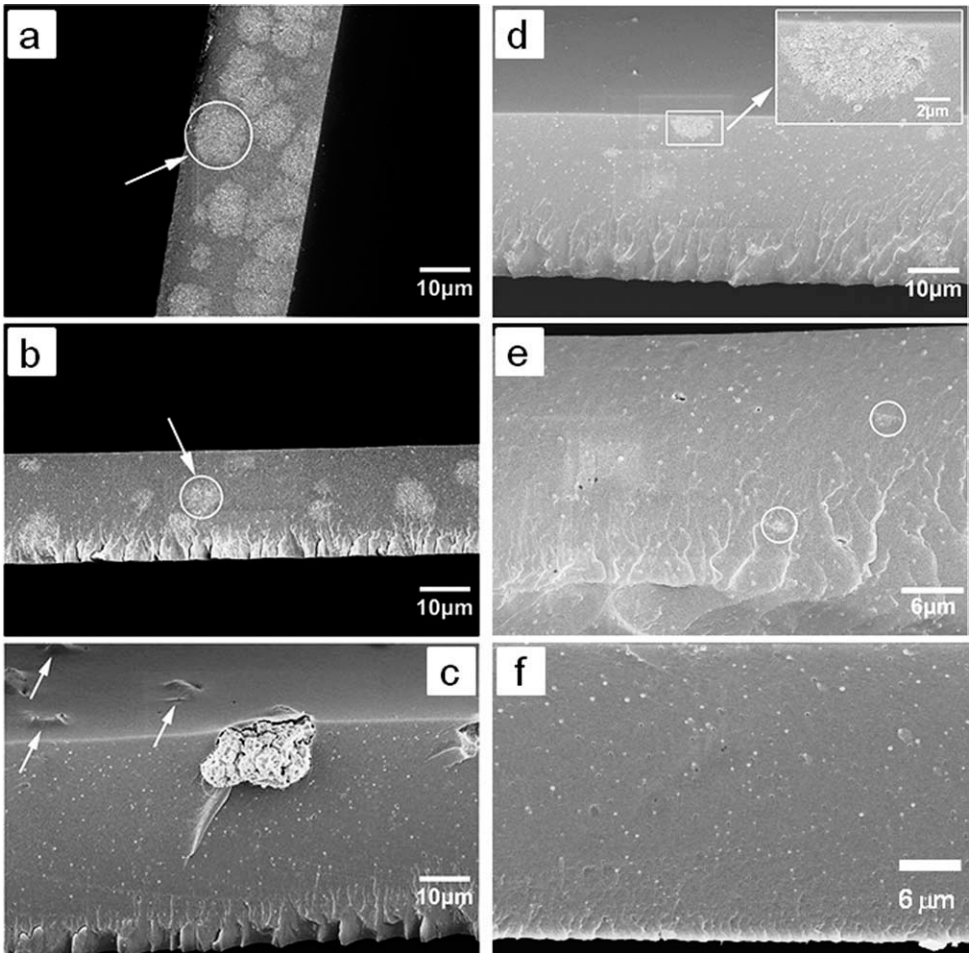

Figure 4 Representative SEM images of the cross-sectional area of various PVDF/PE/ZrX composite membranes, EHT 10 kV. (a) ZrHP 5 wt %, (b) ZrHP 1 wt %, (c) ZrS 5 wt %, (d) ZrO 5 wt %, and (e) ZrO 1 wt %. The circled areas pointed by the arrows in (a) and (b) indicate large clusters of aggregated particles. The arrows in (c) indicate membrane defects created by agglomerates below the membrane surface similar to the one in the front plane of the image. The enclosed areas in (d) and (e) highlight the relatively smaller agglomerates of ZrO. The well-dispersed small particles of about 300–400 nm present in all the images correspond to polyelectrolyte clusters [8].

zirconium-based additives in the PVDF/PE polymer matrix of the composite membranes (Fig. 4). Although low particle loadings (<1%) were homogeneously dispersed [at the level resolvable by SEM, Fig. 4(f)], the particles aggregate and are distributed nonhomogeneously throughout the membrane at high loadings (>1%), Fig. 4(a–e). A critical parameter in the dispersion process is the magnitude of the interparticle forces relative to those between the particles and the suspending medium.[9,33] For instance, unfavorable effects can arise due to the competition between the van der Waals attractions, Coulombic forces, and/or specific polymer-particle and interparticle interactions.[33,34] The aggregation behavior witnessed in the PVDF/PE/ZrX composite membranes at medium and high particle mass fractions may be explained by unfavorable interactions between the hydrophilic surface of the ZrX particles and the hydrophobic polymer matrix. Because of the large surface-to-volume ratio of the particles, this incompatibility is greatly amplified leading to serious aggregation, especially when no surface modifiers or compatibilizers are utilized. Similarly, in the case of ZrO particles, a reduced surface-to-volume ratio because of their crystalline form might explain the better dispersion of this additive at all mass fractions when compared to ZrS and ZrHP [Fig 4(d,e)].

Alternatives to improve the particle dispersion in the PVDF/PE matrices, such as compatibilization and pre-exfoliation of zirconium-based particles via modification with tetra-*n*-butylammonium hydroxide,[16,35] and formation of predispersed particle gels in NMP[36] compatible with the PVDF/PE blends are being considered for future work.

Proton conductivity

The proton conductivity from HTC screening of 45 zirconium-based composite membranes, as well as five PVDF/PE reference membranes, is shown in

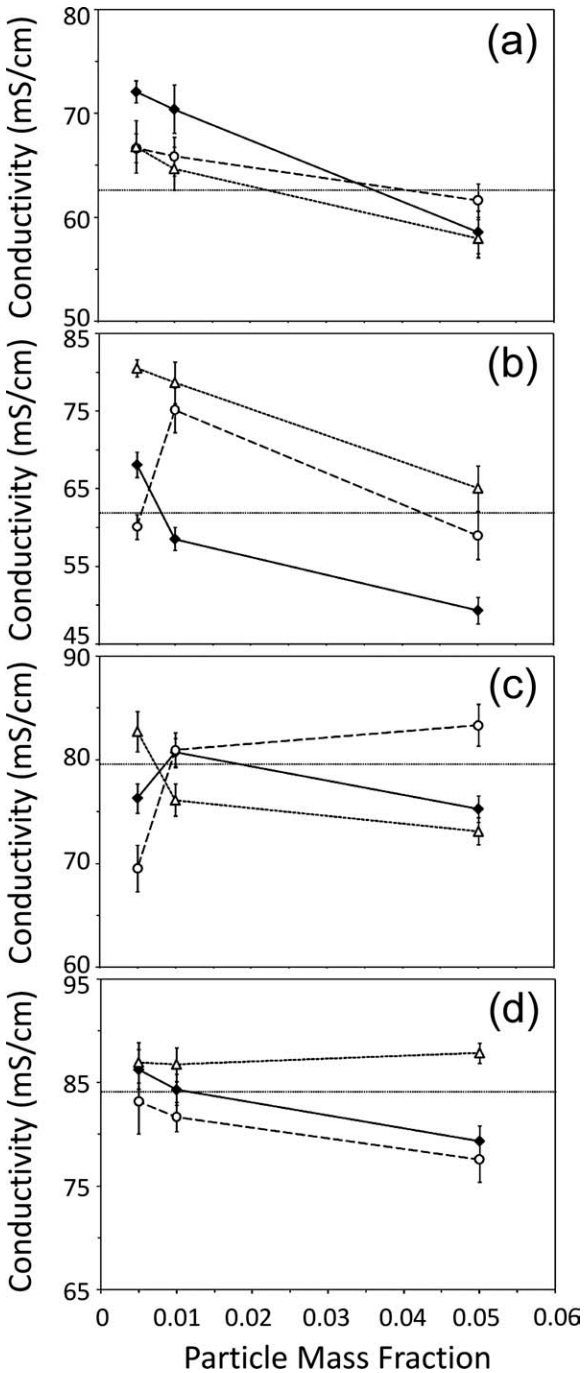

Figure 5 Proton conductivity of PVDF/PE/ZrX composite membranes (ZrHP –◆–, ZrO –○–, ZrS –Δ–) by PVDF grade. (a) Kynar® 500 (b) Kynar® 731, (c) Kynar® 2801, and (d) Kynar® 2821. The horizontal dotted lines (.....) represent reference nonhybrid PVDF/PE membranes for each corresponding PVDF grade. Testing conditions: 18.2 MΩ water at 25°C. Excitation signal: 1000 Hz, 30 mV. Values are presented as averages is ±95% confidence intervals. Data for Kynar® 2851 are available in the Supporting Information.

Figure 5. An initial assessment of the plots reveals higher overall conductivity values for membranes containing PVDF:HFP copolymers, in agreement with our previous study of nonhybrid PVDF/PE PEMs.[8] Proton conductivity is also reduced in composite membranes with high content (≥5 wt %) of particles with respect to corresponding particle-free references, which might be related to particle aggregation and clustering noticed at high particle mass fractions (Fig. 4). Higher conductivity of zirconium-based composites is evidenced at low- to medium particle loadings in composite membranes containing PVDF homopolymers (Kynar® PVDF 500 and 731). To explore this idea, conductivity data from composite membranes was subjected to statistical analysis using an unbalanced GLM. A global analysis of all conductivity data (three-way GLM) revealed statistically significant effects of particle concentration ($F_{(2,1181)} = 54.07$, $P < 0.001$), particle type ($F_{(2,1181)} = 20.64$, $P < 0.001$), and PVDF grade ($F_{(4,1181)} = 172.58$, $P < 0.001$). Figure 6 shows plots of unweighted means of proton conductivity (from the GLM analysis) for the composite membranes as function of particle type and particle mass fraction (both identified as significant factors). The lowest conductivity corresponds to a particle loading of 5 wt %, supporting the idea that the reduction in conductivity is related to aggregation of the solid phase at high particle contents (seen in SEM). In addition, an overall net gain in conductivity is noticed for composite membranes containing 0.5 wt % and 1 wt % zirconium additives (Fig. 6, right), compared to PVDF/PE controls. A clear variation in mean conductivity with particle type is observed (Fig. 6, left), with ZrS yielding higher σ values than ZrO and ZrHP. This behavior is anticipated as the acidity of sulfated zirconia solids is among the strongest of all known solid superacids (Hammet acidity function $H_0 \leq -16.04$).[12,23,37,38] Moreover, the small difference in conductivity noticed between ZrO- and ZrHP-based membranes is in agreement with a slightly improved conductivity observed in ZrO solid acid conductors compared to ZrHP.[13]

In a recent study of PVDF/PE blends, we determined that a direct relationship exists between proton conductivity and the crystalline characteristics of the inert PVDF phase.[8] Particularly, membranes containing PVDF homopolymers with high crystallinity and larger crystallites had lower proton conductivity. To explain this effect, we proposed that sizeable dense PVDF regions, arising from the melting of highly concentrated large crystallites in the homopolymer-based matrix during heating above T_m, precluded the segmental motion and rearrangement of PE chains. This presumably resulted in a semi-interpenetrating network with lower connectivity and thus, reduced conductivity. Interestingly, statistically significant (2-way GLM by PVDF type, $P < 0.05$) conductivity increments resulting from the addition of zirconium-based acid inorganic fillers to PVDF/PE blends occurred only in membranes containing

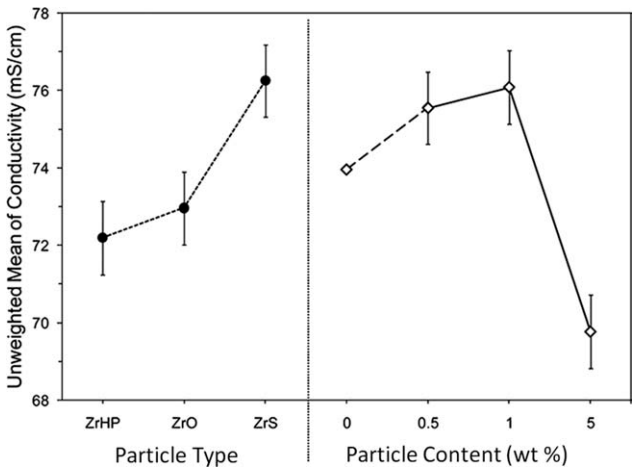

Figure 6 Global unweighted means of conductivity, estimated from and three-way univariate unbalanced GLM analysis (full factorial model), as a function of particle type (left) and particle content (right). Error bars represent the upper and lower bounds of 95% confidence intervals.

PVDF homopolymers (at low- and medium particle loadings) [Fig. 5(a,b)]. Specifically, membranes based on Kynar® 500 exhibited overall conductivity increments of 9.5% and 7%, whereas those containing Kynar® 731 showed improvements of 12.4% and 14.3% at particle contents of 0.5 wt % and 1 wt %, respectively. Surface proton transport is the dominant transport mechanism in solid acids[13] because of exposed acid sites on the surface of the solid that allow the formation of a water layer around the particle where water-assisted transport is occurs. Therefore, the increase in conductivity observed in PVDF homopolymer-based composite membranes is presumably explained by transport along proton-conducting paths provided by the hydration layer of the particles that link nonconnected PE channels. It should also be mentioned that the polar, ionic PE likely forms an adsorbed coating on the hydrophilic particle phase, supporting the transport of protons along the particle surface. Future ultrastructural experiments, e.g., TEM, will be aimed at evaluating the relative sizes and connectivity of particle, PVDF, and PE domains to evaluate this tentative structure–property relationship.

Conductivity of PVDF:HFP copolymer-based composite membranes at low- and medium particle loadings was either slightly lower than or not statistically different from nonhybrid counterparts (two-way GLM by PVDF type, $P > 0.05$). The latter case suggests that the ZrX additives do not alter considerably the local dynamics of water molecules in copolymer-based films. A similar effect has been noticed in Nafion® membranes containing zirconium phosphate filler, where the local dynamics of water molecules in the composite membrane is quite similar to that of simple hydrated Nafion®.[39] The case of reduced conductivity may be explained by an increment of diffusional resistance as particles occupy the volume that would otherwise correspond to proton conducting channels. The lack of a defined trend of

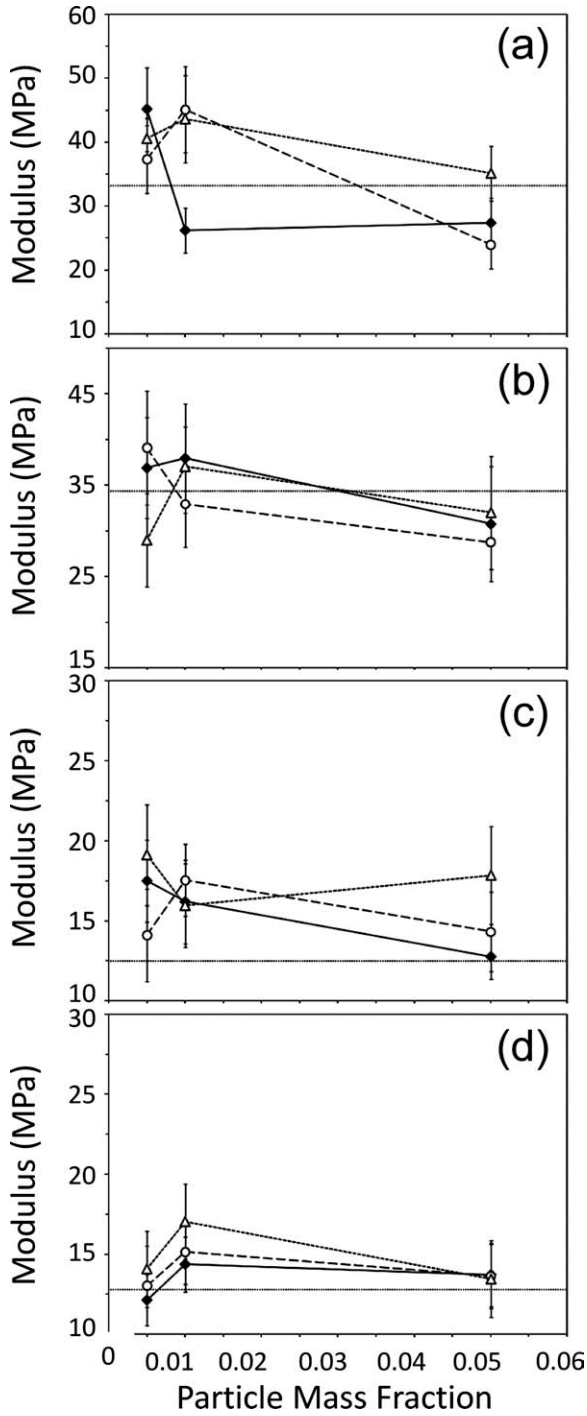

Figure 7 Elastic modulus (biaxial) of PVDF/PE/ZrX composite membranes (ZrHP –◆–, ZrO –○–, ZrS –Δ–) by PVDF grade. (a) Kynar® 500 (b) Kynar® 731, (c) Kynar® 2801, and (d) Kynar® 2821. The horizontal dotted lines (.....) represent reference nonhybrid PVDF/PE membranes for each corresponding PVDF grade. Values are presented as averages ±95% confidence intervals. Data for Kynar® 2851 are available in the Supporting Information.

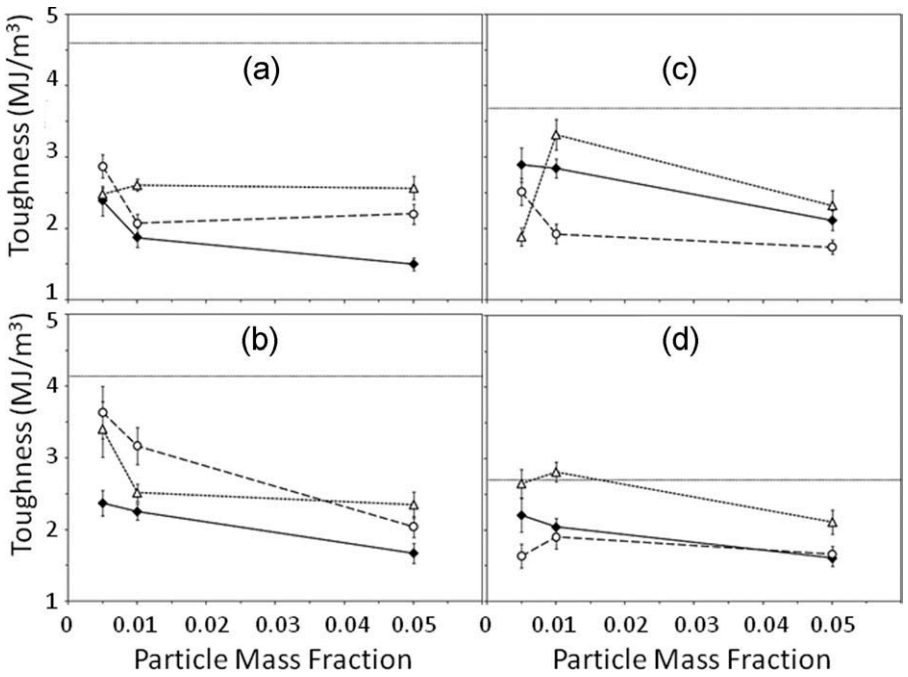

Figure 8 Toughness (biaxial) of PVDF/PE/ZrX composite membranes (ZrHP –◆–, ZrO –○–, ZrS –Δ–) by PVDF grade. (a) Kynar® 500 (b) Kynar® 731, (c) Kynar® 2801, and (d) Kynar® 2821. The horizontal dotted lines (.....) represent reference nonhybrid PVDF/PE membranes for each corresponding PVDF grade. Values are presented as averages ±95% confidence intervals. Data for Kynar® 2851 are available in the Supporting Information.

these conditions at different particle contents further emphasizes the suboptimal particle dispersion within the PVDF/PE matrices (even at low particle loadings) that was highlighted in the previous section. These results illuminate the need for particle modification and/or pre-exfoliation approaches. The very few cases where high ZrX mass fraction resulted in enhanced conductivity in the copolymer-based PVDF/PE films [Fig. 5(b–d)] might be explained by the fortuitous formation of particle–particle paths from contiguous particle agglomerates that connect the external faces of the membrane.

Mechanical properties

Controlling the amount of inorganic additives and their degree of dispersion in a polymer matrix are fundamental factors influencing elastic modulus and toughness of composite membranes. The elastic modulus and toughness of the composite membranes as a function of particle mass fraction are shown in Figures 7 and 8, respectively. Statistical analysis revealed significant effects of particle content ($F_{(2,1105)} = 37.19$, $P < 0.001$), particle type ($F_{(2,1105)} = 11.3$, $P < 0.001$), and PVDF grade ($F_{(4,1105)} = 249.52$, $P < 0.001$) on membrane elastic modulus; however, the "practical" effect of particle content and type is weak in comparison to the effect of PVDF grade ($\eta_{p,\text{content}}^2 \leq 0.06$ vs. $\eta_{p,\text{grade}}^2 = 0.48$, where η_p^2 is the partial eta squared statistic). This is expected as the PVDF support matrix controls the tensile properties to the membranes. Likewise, significant effects of particle content ($F_{(2,1105)} = 221.58$, $P < 0.001$), particle type ($F_{(2,1105)} = 129.94$, $P < 0.001$), and PVDF grade ($F_{(4,1105)} = 66.05$, $P < 0.001$) on membrane toughness were identified; however, contrary to their small effect on the membrane elastic modulus, the particle type and content have an important effect on toughness. Generally, the size of particles is too small to provide toughening through a crack-bridging mechanism, and they cannot effectively enhance crack trajectory tortuosity[40]; therefore, the strong effect of particle type and content on toughness may be related to factors such as membrane stiffening and/or stress-absorbing defect sites arising from the insertion of particles.

Despite the reduced effect of particle content, compared to that of PVDF grade, on the membrane elastic modulus, a reinforcing effect with respect to nonhybrid membranes is evidenced at low- to medium particle loadings. The effect is especially manifested in the modulus of composite membranes containing flexible PVDF:HFP copolymers (statistically significant, two-way GLM by PVDF type, $P < 0.05$), thus suggesting an increment in membrane stiffness. On the contrary, toughness diminished for all composite membranes at all loadings, (statistically significant, two-way GLM by PVDF type, $P < 0.001$), presumably due to the abovementioned membrane stiffening and high density of membrane defects due to solid-phase aggregation at high loadings (Fig. 4). To further visualize the effect of inorganic zirconium-

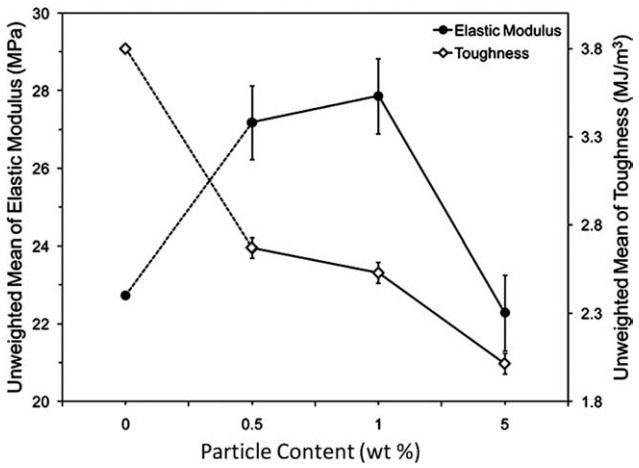

Figure 9 Global unweighted means of elastic modulus and toughness, estimated from three-way univariate unbalanced GLM analysis (full factorial model), as a function of particle content. Error bars represent the upper and lower bounds of 95% confidence intervals.

based fillers on the mechanical properties of composite membranes, the global unweighted means of elastic modulus and toughness are presented in Figure 9. A clear reinforcing stiffening effect with respect to reference PVDF/PE membranes, characterized by an overall elastic modulus increase of 19.5% and 22.5%, is evidenced at particle loadings of 0.5 wt % and 1 wt %, respectively. This stiffening correlates well with the observed overall reduction in membrane toughness (29.7% and 33.4% decline) at identical particle composition. These results are in accordance with the mechanical behavior observed in other organic/inorganic systems where nanocomposites stiffen efficiently but tend to fail prematurely as a result of toughness reduction.[33,40] Moreover, similar outcomes have been observed in poly(arylene ether sulfone)-based PE systems that incorporate zirconium hydrogen phosphate particles.[15]

The abrupt reduction in the overall elastic modulus (22.5% increase to 2% decrease) and further toughness decline (33.4 to 46.9% reduction) at the transition from medium to high particle loadings confirm the formation of membrane defects derived from particle agglomerates that adversely affect the energy absorption capability of the membrane during mechanical deformation.

CONCLUSIONS

Proton-conducting triphase composite membranes were fabricated by incorporating zirconium oxide, zirconium hydroxide sulfate, and zirconium hydrogen phosphate particles into polymeric blends of Kynar® and a cross-linked sulfonated acrylic PE. The proton conductivity and mechanical properties of the membranes were assayed by means of EIS and biaxial axisymmetric deformation high-throughput screening tools. Compared to nonhybrid PVDF/PE reference membranes, the resulting composite membranes exhibited improved conductivity (7 to 14% increase) at 0.5 to 1 wt % particle loadings. A particular beneficial "defect healing" effect of the ZrX fillers was observed in composite membranes prepared from highly crystalline PVDF homopolymers (i.e., Kynar® 500 and 731). We tentatively propose that the hydration layer of the embedded particles constitutes a proton-conducting route that allows the interconnection of PE channels previously separated by dense PVDF areas resulting from large PVDF crystallites. This hypothesis suggests that future ultrastructural experiments, e.g., TEM, are warranted to evaluating the relative sizes and connectivity of particle, PVDF, and PE domains to evaluate the tentative structure–property relationship. Tensile properties were similarly enhanced by the insertion of ZrX fillers, especially in membranes containing more flexible PVDF:HFP copolymers (i.e., Kynar® 2801, 2821, and 2851) where a reinforcing stiffening effect (20% elastic modulus increment) was evident at 0.5 to 1 wt % particle loadings. This increment in the elastic modulus was, however, detrimental for membrane toughness throughout the whole range of PVDF grades and particle loadings. Particle dispersion was limited by apparently unfavorable particle–polymer interactions resulting in severe aggregation at high particle contents ($\geq$5 wt %). Because the degree of particle dispersion is critical for modulus and strength development, all mechanical properties were significantly lessened at high particle loadings. Proton conductivity was similarly affected as instead of providing an internal scaffold that stabilizes and enhances the ionic cluster volume, aggregated particles resulted in increased diffusional resistance by occupying the volume otherwise corresponding to proton-conducting channels.

As a proof of concept of incorporating proton-conducting inorganic fillers to physically blended polymers, the results obtained herein are encouraging. Addressing particle dispersion issues by perhaps forming predispersed zirconium-based particle gels in NMP that are compatible with both the PVDF and neutralized PE solutions, and/or using acrylic PEs of significantly lower equivalent weight and higher conductivity,[8] may result in promising alternative PEMs.

References

1. Barbir, F. Energy 2009, 34, 308.
2. Neef, H.-J. Energy 2009, 34, 327.
3. Sopian, K.; Daud, W. R. W. Renew Energy 2006, 31, 719.
4. U.S. Department of Energy Office of Science Basic Research Needs for the Hydrogen Economy: Report of the Basic Energy

Sciences Workshop on Hydrogen Production, Storage, and Use. Washington DC. 2004; p 178.
5. Hickner, M. A.; Ghassemi, H.; Kim, Y. S.; Einsla, B. R.; McGrath, J. E. Chem Rev 2004, 104, 4587.
6. Dobrovol'skii, Y. A.; Volkov, E. V.; Pisareva, A. V.; Fedotov, Y. A.; Likhachev, D. Y.; Rusanov, A. L. Russ J Gen Chem 2007, 77, 766.
7. Meier-Haack, J.; Taeger, A.; Vogel, C.; Schlenstedt, K.; Lenk, W.; Lehmann, D. Sep Purificat Technol 2005, 41, 207.
8. Zapata, P.; Mountz, D.; Meredith, J. C. Macromolecules 2010, 43, 7625.
9. Scherer, G. G. Fuel Cells I; Springer-Verlag: Berlin Heidelberg, 2008; Vol. 215, p 268.
10. Savadogo, O. J Power Sources 2004, 127, 135.
11. Neburchilov, V.; Martin, J.; Wang, H.; Zhang, J. J Power Sources 2007, 169, 221.
12. Thampan, T. M.; Jalani, N. H.; Choi, P.; Datta, R., J Electrochem Soc 2005, 152, A316.
13. Hogarth, W. H. J.; Costa, J. C. D. d.; Lu, G. Q. M. J Power Sources 2005, 142, 223.
14. Kim, J.-D.; Mori, T.; Honma, I. J Electrochem Soc 2006, 153, A508.
15. Hill, M. L.; Kim, Y. S.; Einsla, B. R.; McGrath, J. E. J Membr Sci 2006, 283, 102.
16. Kuan, H.-C.; Wu, C.-S.; Chen, C.-Y.; Yu, Z.-Z.; Dasari, A.; Mai, Y.-W. Electrochem Solid-State Lett 2006, 9, A76.
17. Bi, C.; Zhang, H.; Zhang, Y.; Zhu, X.; Ma, Y.; Dai, H.; Xiao, S. J Power Sources 2008, 184, 197.
18. Tchicaya-Bouckary, L.; Jones, D. J.; Rozière, J. Fuel Cells 2002, 2, 40.
19. Alberti, G.; Casciola, M.; Pica, M.; Tarpanelli, T.; Sganappa, M. Fuel Cells 2005, 5, 366.
20. Gaowen, Z.; Zhentao, Z. J Membr Sci 2005, 261, 107.
21. Alberti, G.; Casciola, M. Ann Rev Mater Res 2003, 33, 129.
22. Hogarth, W. H. J.; Costa, J. C. D. d.; Drennan, J.; Lu, G. Q. M. J Mater Chem 2005, 15, 754.
23. Tominaka, S.; Akiyama, N.; Croce, F.; Momma, T.; Scrosati, B.; Osaka, T. J Power Sources 2008, 185, 656.
24. Zapata, P.; Basak, P.; Meredith, J. C. Electrochim Acta 2009, 54, 3899.
25. Sormana, J.-L.; Chattopadhyay, S.; Meredith, J. C. Rev Sci Instrum 2005, 76, 062214.
26. Meredith, J. C.; Karim, A.; Amis, E. J. MRS Bull 2002, 27, 330.
27. Tatsumi, T.; Matsuhashi, H.; Arata, K. Bull Chem Soc Jpn 1996, 69, 1191.
28. Ludmány, A.; Kurek, S. S.; Stoklosa, A.; Wilczynski, G.; Wójtowicz, A.; Zajecki, J. Appl Catal A: Gen 2004, 267, 149.
29. Kumar, G. G.; Kim, P.; Nahm, K. s.; Elizabeth, R. N. J Membr Sci 2007, 303, 126.
30. Rajendran, S.; Sivakumar, P.; Babu, R. S. Bull Mater Sci 2006, 29, 673.
31. Mhalgi, M. V.; Khakhar, D. V.; Misra, A. Polym Eng Sci 2007, 47, 1992.
32. Gregorio, R. J. J Appl Polym Sci 2006, 100, 3272.
33. Goettler, L. A.; Lee, K. Y.; Thakkar, H. Polym Rev 2007, 47, 291.
34. Hooper, J. B.; Schweizer, K. S.; Desai, T. G.; Koshy, R.; Keblinski, P. J Chem Phys 2004, 121, 6986.
35. Sun, L.; Boo, W. J.; Sun, D.; Clearfield, A.; Sue, a. H.-J. Chem Mater 2007, 19, 1749.
36. Casciola, M.; Alberti, G.; Donnadio, A.; Pica, M.; Marmottini, F.; Bottino, A.; Piaggio, P. J Mater Chem 2005, 15, 4262.
37. Eley, D. D.; Pines, H.; Weisz, P. B. Advances in Catalysis; Academic Press, Inc.: San Diego, 1990; Vol. 37, p 329.
38. Fraenkel, D. Chem Lett 1999, 28, 917–918.
39. Paciaroni, A.; Casciola, M.; Cornicchi, E.; Marconi, M.; Onori, G.; Pica, M.; Narducci, R.; Francesco, A. D.; Orecchini, A. J Phys: Condens Matter 2006, 18, S2029.
40. Zerda, A. S.; Caskey, T. C.; Lesser, A. J. Macromolecules 2003, 36, 1603.